Fatigue Life Prediction of Composite Adhesive Joints using LS-DYNA®

Ala Tabiei* and Wenlong Zhang*
*Department of Mechanical and Materials Engineering, University of Cincinnati, Cincinnati, Ohio 45221, USA

Abstract

Composite and adhesive joints are used increasingly in the automotive industry and an active research area is the fatigue analysis of adhesive joints. In this paper, a methodology to predict the fatigue life of adhesive joint is proposed and implemented into LS-DYNA with the joint modeled using a user-defined cohesive material. Fatigue crack growth rate is used to obtain the fatigue damage accumulation rate in cohesive zone model. Our method is verified by numerical simulations of two commonly used adhesive joints in the automotive industry: single lap joint and stepped lap joint. The predicted S-N curve fits well with the experimental data.

1. Introduction

Adhesive joint can not only be used between composite materials but also be used to connect composite to metal, and metal to metal. It has the advantage of lower weight, lower fabrication cost, eliminating stress concentration, increasing corrosion resistance and more design flexibility. It also increases the overall stiffness of the body because of its continuous nature, thus enabling thinner materials to be used [1]. In structural applications, adhesive joints are primarily designed to carry shear load. Thus the commonly used adhesive joint types are single lap joint, double lap joint, strapped joint, and compound joint [2].

Despite all these advantages of adhesive joints, there remains a concern in the industry that is the long-term service life under cyclic loading conditions. Prediction of fatigue life is especially important for parts near the engine where vibration is intense. Fatigue life prediction is needed so a replacement can be done before that part fails. A Large amount of research has been done in this area [3-7]. Apart from the experimental studies about the influence of various factors like temperature [8], adhesive thickness [9], vibration frequency [10] and load ratio [11], a substantial amount of numerical studies also emerge to predict the fatigue life of adhesive joints [12-15]. Most of them use the cohesive zone model combined with fracture mechanics and damage mechanics to simulate fatigue accumulation. Roe (2003) [12] proposed a damage evolution law to predict fatigue accumulation. By integrating the damage accumulation rate over time, the amount of damage is obtained and used to decrease the cohesive strength. Roe's damage evolution law provides insight into how damage mechanics can be utilized for fatigue analysis but also suffers from the high computational cost when it is high cyclic loading, because a history of deformation rate is needed for damage calculation.

When it comes to high cyclic loading, a commonly used approach is to combine damage accumulation with fracture toughness and fatigue crack growth rate (FCGR), which is often characterized by Paris law [16]. Paris law defines the relationship between crack propagation rate and fracture toughness range, as shown in Equation 1:

$$\frac{da}{dN} = D(\Delta K)^B, \text{where } \Delta K = K_{max} - K_{min} \quad (1)$$

where a is the crack length and N is the number of loading cycles. D and B are curve fitting parameters of experiment data, and they can be considered as material parameters. Since correlation can be found between energy release rate and fracture toughness, Paris law can also be expressed in terms of energy release rate change (Equation 2), as shown in Figure 1.

$$\frac{da}{dN} = C(\Delta G)^m, \text{where } \Delta G = G_{max} - G_{min} \quad (2)$$

After the Paris law relationship is defined by experiment, the fatigue crack growth rate can be implemented into finite element scheme with the help of cohesive zone model, and this will be described in detail in Section 2.

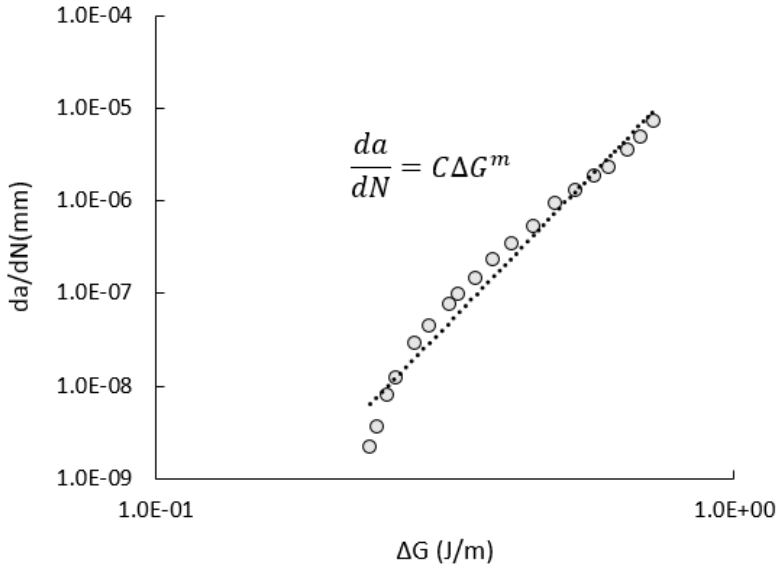

Figure 1. Typical Paris law

Cohesive zone model was proposed by Dugdale (1960) [17] and Barenblatt (1962) [18] to handle the process zone near the crack tip (Figure 2). It describes the traction separation relationship between two surfaces before they are formed. The traction-separation relationship is often called cohesive law, and the area under traction-separation curve corresponds to the critical energy release rate it takes to create a new pair of surfaces. Cohesive zone model is often implemented with cohesive elements, which can have small and even zero thickness without reducing the critical time step. That is because only stiffness and mass are used for the time step calculation. This feature gives it advantages in modeling adhesives whose thickness is usually very small. A detailed formulation about cohesive element can be found in [19].

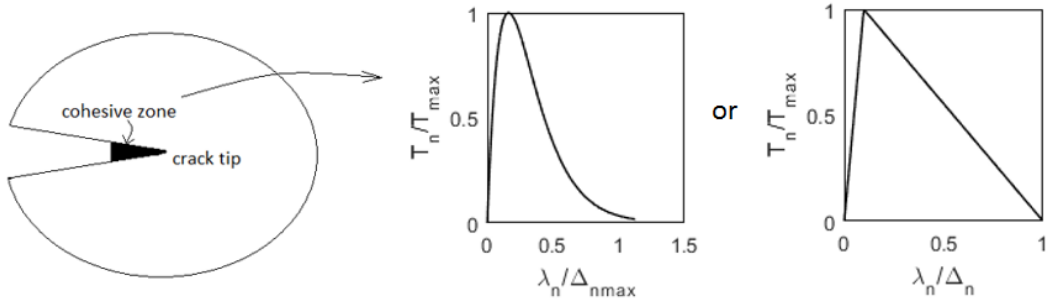

Figure 2. Illustration of cohesive zone model and different cohesive laws

For high cyclic fatigue, algorithms like cyclic jump method, linear extrapolation method has been proposed by authors to reduce the high computational cost. A better choice is to use implicit time integration combined with these algorithms because it is unconditionally stable and the time step can be as big as needed. However, cohesive laws have a turning point in the traction-separation curve, and it makes it hard to achieve convergence, and some techniques like arc length method [20] and viscous regularization [21] need to be used to overcome that difficulty.

In this paper, a method to predict fatigue life using fatigue crack growth rate and cohesive model is proposed. The joint is modeled using a user-defined cohesive material model. Implicit time integration scheme is used, and viscous regularization algorithm is programmed within the user-defined material model to help convergence. This cohesive damage model is used to predict S-N curve of single lap adhesive joint and stepped lap adhesive joint, which is commonly utilized in the automotive industry. This paper is organized as follows: In section 2, the methodology and its implementation into LS-DYNA are presented; In section 3, two numerical simulations are carried out to verify our proposed method. Paris law parameters used in our simulation are obtained from experiments in literature.

2. Combining Fatigue Crack Growth Rate (FCGR) with Cohesive Zone Model

The approach of combining FCGR with cohesive zone model has been used by several authors [13-15]. Turon (2006) [13] derived overall damage accumulation rate $\dot{d}$ from the relationship of total damage parameter $d = d_s + d_\mathrm{f}$ and the area covered by cyclic loading curve in traction-separation law. Harper (2010) [14] derived fatigue damage accumulation rate $\dot{d}_\mathrm{f}$ by proposing a concept of fatigue crack length across the element, and Landry (2012) [15] used the same concept to derive the fatigue damage accumulation rate. These papers provide insight for relating the $\dot{d}_\mathrm{f}$ to FCGR. These models were proposed for delamination fatigue analysis, where at the crack tip cohesive elements are at the descending part of the cohesive law, so these models did not account for the fatigue accumulation when it is in the ascending part of the cohesive law. For adhesive joints, however, when at service load, it should be way below the ultimate strength for most part of adhesive joint, thus in the elastic ascending part of cohesive law. Thus, the fatigue accumulation during that period, should also be considered when modeling adhesive joints, and that issue is addressed in this paper. In our method, different from other authors, a new way of relating FCGR to the damage parameter is used, and damage parameter is used to reduce the critical energy release rate in the cohesive zone model. Bilinear cohesive law is used as it is straightforward and robust in cyclic loading.

2.1.Bilinear cohesive law

Bilinear cohesive law by Camanho (2003) [22] uses a B-K (1997) mixed mode criterion [23] to combine mode I and mode II loading into mixed mode loading and to guarantee the continuity of traction-separation curve under arbitrary cyclic loading (Figure 3). For cohesive law, mode I loading corresponds to loading in the normal direction of the surface, and mode II loading corresponds to the tangential loading on the surface. For static loading, the damage parameter is expressed in Equation 3 [24].

$$d_s = \min\left(\frac{\Delta^F}{\lambda_{max}}\frac{\lambda_{max}-\Delta^0}{\Delta^F-\Delta^0}, 1\right) \tag{3}$$

Where

$$\Delta^0 = \Delta_I^0\Delta_{II}^0\sqrt{\frac{1+\beta^2}{\left(\Delta_{II}^0\right)^2+\left(\beta\Delta_I^0\right)^2}} \tag{4}$$

$$\Delta^F = \begin{cases} \dfrac{2\left(1+\beta^2\right)}{\Delta^0}\left[\left(\dfrac{EN}{G_{IC}}\right)^\alpha+\left(\dfrac{ET\beta^2}{G_{IIC}}\right)^\alpha\right]^{-1/\alpha} & \lambda_I > 0 \\ \dfrac{2G_{IIC}}{S} & \lambda_\mathrm{I} \le 0 \end{cases} \tag{5}$$

$$\Delta_I^0 = T/EN \tag{6}$$

$$\Delta_{II}^{0} = S/ET \tag{7}$$

In these equations, Δ^F represents the mixed mode separation, exceeds which the cohesive zone will fail; Δ^0 represents the mixed mode separation that corresponds to the maximum traction; $\lambda_{max} = \sqrt{\lambda_I^2 + \lambda_{II}^2}$ is the maximum mixed mode separation within a loading cycle; $\beta = \lambda_{II}/\lambda_I$ is the mixed mode ratio, in which λ_I is the separation in normal direction and λ_{II} is the separation in tangential direction; T and S are the cohesive strength in normal and tangential direction respectively; EN and ET are the initial stiffness in normal and tangential direction respectively; G_{IC} and G_{IIC} are the critical energy release rate in mode I and mode II respectively. α in Equation 5 is an adjustable parameter defined by users and if it is taken as 1, which means a linear law is used to combine mode I and mode II deformation, Equation 3 becomes:

$$\Delta^F = \begin{cases} \dfrac{2\left(1+\beta^2\right)}{\delta^0}\left[\left(\dfrac{EN}{G_{IC}}\right)+\left(\dfrac{ET\beta^2}{G_{IIC}}\right)\right]^{-1} & \lambda_{\mathrm{I}} > 0 \\ \dfrac{2G_{IIC}}{S} & \lambda_{\mathrm{I}} \le 0 \end{cases} \tag{8}$$

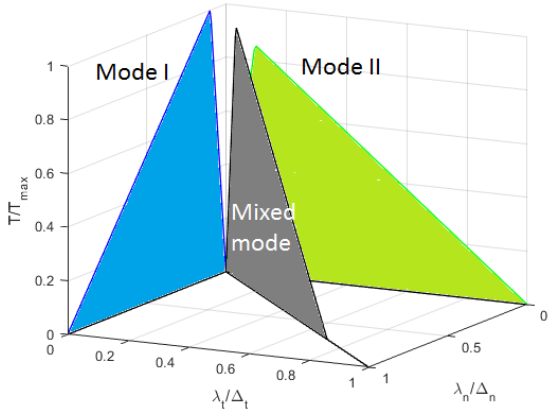

Figure 3. Illustration of bilinear cohesive law

After the static damage parameter d_s is defined, tractions in normal and tangential direction can be defined as:

$$T_n = \begin{cases} EN \times (1-d_s) \times \lambda_{\mathrm{I}} & 0 < \lambda_{\mathrm{I}} < \Delta^F \\ EN \times Scale\ Factor \times \lambda_{\mathrm{I}} & \lambda_{\mathrm{I}} < 0 \end{cases} \tag{9}$$

$$T_t = ET \times (1-d_s) \times \lambda_{\mathrm{II}} \tag{10}$$

When fatigue damage factor d_f is considered, we need to consider its influence on the damage parameter and it will become $d = d_s + d_f$ and Equation (9-10) becomes:

$$T_n = \begin{cases} EN \times (1-d_s-d_{\mathrm{f}}) \times \lambda_{\mathrm{I}} & 0 < \lambda_{\mathrm{I}} < \Delta^F \\ EN \times Scale\ Factor \times \lambda_{\mathrm{I}} & \lambda_{\mathrm{I}} < 0 \end{cases} \tag{11}$$

$$T_t = ET \times (1-d_s-d_{\mathrm{f}}) \times \lambda_{\mathrm{II}} \tag{12}$$

The effect of fatigue damage on Equation (11-12) can be illustrated in Figure 4.

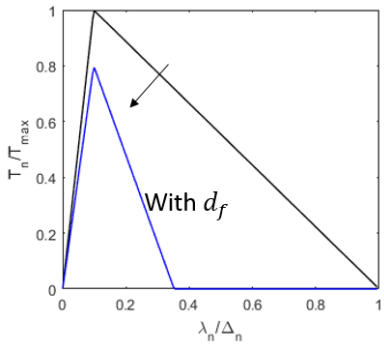

Figure 4. Illustration of fatigue effect on bilinear cohesive law

2.2. Damage accumulation rate

As stated in the previous sub-section, when fatigue is considered, the damage parameter becomes $d = d_s + d_f$. Since static damage parameter d_s will not change with cyclic loading, the main objective becomes to calculate d_f by integrating the fatigue damage accumulation rate $\dot{d}_f$ over time. Inspired by Turon's approach [13], we use the ratio between damaged area to the overall area in an element A_d/A_e to obtain $\dot{d}_f$. When an element is in the cohesive zone, A_d/A_e can be represented Equation 13:

$$\frac{A_d}{A_e} = \frac{S+F}{G_c - R} \tag{13}$$

Where S, F, and R are the areas under cohesive law illustrated in Figure 5(a). S represents the static damage, and F accounts for the fatigue damage.

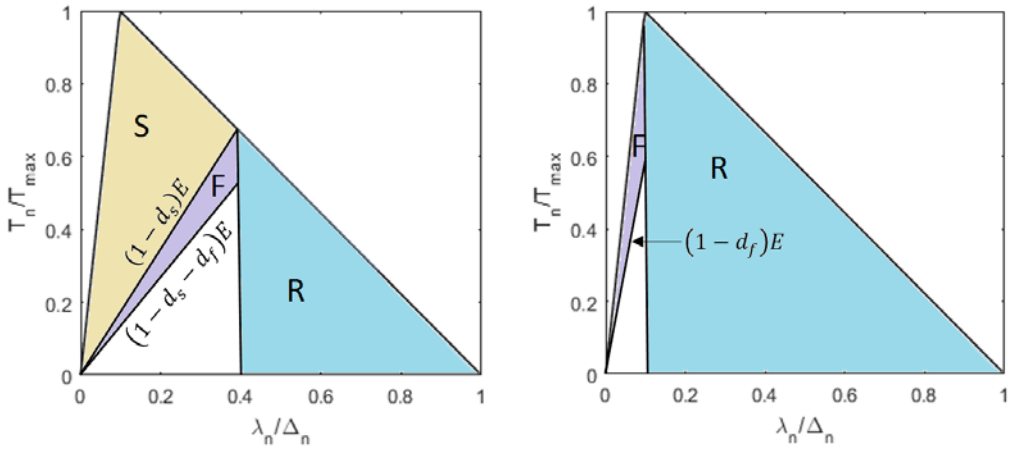

(a) (b)

Figure 5. Static and fatigue damaged area in cohesive law (a) when separation is at descending part (b) when separation is at ascending part

$$S = \frac{1}{2}E\Delta_0\Delta_f - \frac{1}{2}E(1-d_s)\lambda\Delta_f \tag{14}$$

$$G_c = \frac{1}{2}E\Delta_0\Delta_f \tag{15}$$

$$R = \frac{1}{2}E(1-d_s)\lambda\left(\Delta_f - \lambda\right) \tag{16}$$

$$F = \frac{1}{2}E(1-d_s)\lambda^2 - \frac{1}{2}E\left(1-d_s-d_f\right)\lambda^2 \tag{17}$$

In Equation (14-17), E represents either EN or ET, depending on whether it is normal or tangential loading. Δ_f and Δ_0 could also represent the characteristic separations in normal or tangential direction, in which Δ_f is the maximum allowable separation and Δ_0 is the separation at maximum traction. Plug Equation (14-17) back to Equation 13, we will get:

$$\frac{A_d}{A_e} = \frac{\Delta_0\Delta_f - (1-d_s)\lambda\Delta_f + (1-d_s)\lambda^2 - \left(1-d_s-d_f\right)\lambda^2}{\Delta_0\Delta_f - (1-d_s)\lambda\left(\Delta_f-\lambda\right)} \tag{18}$$

where λ is the separation in mixed mode. By ignoring the influence of fatigue accumulation on static damage parameter, the damage accumulation rate can be expressed as:

$$\frac{\partial d}{\partial N} = \frac{\partial d}{\partial A_d}\frac{\partial A_d}{\partial N} = \frac{\partial\left(d_s+d_f\right)}{\partial A_d}\frac{\partial A_d}{\partial N} = \frac{\partial d_f}{\partial A_d}\frac{\partial A_d}{\partial N} = \frac{\partial d_f}{\partial N} \tag{19}$$

From Equation 18 we can get:

$$\frac{\partial d_f}{\partial A_d} = \frac{1}{A_e}\frac{\Delta_0\Delta_f - (1-d_s)\lambda\left(\Delta_f-\lambda\right)}{\lambda^2} \tag{20}$$

The increase of the damaged area along a crack front is equal to the sum of the damaged area increase of all the elements ahead of the crack tip. If the modeling of adhesive joint is using a constant element size, and since the damage at the crack front is approximately uniformly distributed through the width, we can assume that the damaged area of elements in cohesive zone is approximately the same, and the fatigue crack growth rate can be written as:

$$\frac{\partial A}{\partial N} = \frac{A_{cz}}{A_e}\frac{\partial A_d}{\partial N} \tag{21}$$

where A_{cz} is the cohesive zone size. For mode I case [25]:

$$A_{cz,I} = b\frac{9\pi}{32}\frac{EG_{IC}}{T^2} \tag{22}$$

Plug Equation (20-22) into Equation 19, we can get:

$$\frac{\partial d_f}{\partial N} = \frac{32T^2}{b9\pi EG_{IC}}\frac{\Delta_0\Delta_f - (1-d_s)\lambda_I\left(\Delta_f-\lambda_I\right)}{\lambda_I^2}\frac{\partial A}{\partial N} \tag{23}$$

Assuming the adhesive joint has the same width across the section, it can be further simplified to:

$$\frac{\partial d_f}{\partial N} = \frac{32T^2}{9\pi EG_{IC}}\frac{\Delta_0\Delta_f - (1-d_s)\lambda_I\left(\Delta_f-\lambda_I\right)}{\lambda_I^2}\frac{\partial a}{\partial N} \tag{24}$$

where a is the crack length. Similarly, for mode II case the cohesive zone size can be approximated as: [26]

$$A_{cz,II} = \frac{bEG_{IIC}}{S^2} \tag{25}$$

In Mode II case the fatigue damage accumulation rate $\dot{d}_f$ would be:

$$\frac{\partial d_f}{\partial N} = \frac{S^2}{EG_{IIC}}\frac{\Delta_0\Delta_f - (1-d_s)\lambda_{II}\left(\Delta_f-\lambda_{II}\right)}{\lambda_{II}^2}\frac{\partial a}{\partial N} \tag{26}$$

When it is at mixed mode loading case, linear interpolation is used to get the equivalent cohesive zone length:

$$A_{cz} = A_{cz,I} + \beta\left(A_{cz,II} - A_{cz,I}\right) \tag{27}$$

where $\beta = \lambda_{II}/\lambda_I$ is the mixed mode ratio. Then for mixed mode separation, $\dot{d}_f$ becomes:

$$\frac{\partial d_f}{\partial N} = \frac{b}{A_{cz}}\frac{\Delta_0\Delta_f - (1-d_s)\lambda\left(\Delta_f-\lambda\right)}{\lambda^2}\frac{\partial a}{\partial N} \tag{28}$$

where λ is the mixed mode separation. Equation 24, 26 and 28 all represent the $\dot{d}_f$ expression when the separation is at the descending part of cohesive law.

For cases where separation is at the ascending part of cohesive zone ($0 < \lambda < \Delta_0$), like shown in Figure 5(b), a similar approach is used to obtain $\dot{d}_f$. We have $d_s = 0$ and

$$\frac{A_d}{A_e} = \frac{F}{F+R} = \frac{\frac{1}{2}E\lambda^2 - \frac{1}{2}E(1-d_f)\lambda^2}{\frac{1}{2}E\lambda^2} = d_f \tag{29}$$

$$\frac{\partial d_f}{\partial A_d} = \frac{1}{A_e} \tag{30}$$

For mode I:

$$\frac{\partial d_f}{\partial N} = \frac{b}{A_{cz,I}}\frac{\partial a}{\partial N} = \frac{32T^2}{9\pi E G_{IC}}\frac{\partial a}{\partial N} \tag{31}$$

For mode II:

$$\frac{\partial d_f}{\partial N} = \frac{b}{A_{cz,II}}\frac{\partial a}{\partial N} = \frac{S^2}{E G_{IIC}}\frac{\partial a}{\partial N} \tag{32}$$

For mixed mode:

$$\frac{\partial d_f}{\partial N} = \frac{b}{A_{cz}}\frac{\partial a}{\partial N} \tag{33}$$

After the relationship between damage accumulation rate and fatigue crack growth rate is determined, we can relate it to the FCGR:

$$\frac{\partial a}{\partial N} = C(\Delta G)^m \tag{34}$$

Parameters C and m for mode I and mode II can both be determined through experiment. The right-hand side of the equation is energy release rate change, which corresponds to the area under the traction separation law as shown in Figure 6. If the load ratio is known, the energy release rate can be calculated using Equation 35:

$$\Delta G = \frac{1}{2E}(T_{max}^2 - T_{min}^2) = \frac{T_{max}^2}{2E}(1-R^2) \tag{35}$$

Regarding separation in normal and tangential direction, Equation 35 can be represented as:

$$\Delta G_i = \frac{E\lambda_i^2}{2}(1-R^2)(1-d_s)\left(1-d_f\right) \quad i = 1,2 \tag{36}$$

where $i = 1,2$ represents mode I and mode II respectively. Mixed mode energy release rate change is obtained by linear interpolation of mode I and mode II.

$$\Delta G = \Delta G_I + \beta(\Delta G_{II} - \Delta G_I) \tag{37}$$

After that, linear interpolation is used to obtain the mixed mode FCGR parameters:

$$ln(C) = ln(C_{II}) + [ln(C_I) - ln(C_{II})]\left(1 - \frac{G_{II}}{G_T}\right) \tag{38}$$

$$m = m_I + (m_{II} - m_I)\left(\frac{G_{II}}{G_T}\right) \tag{39}$$

Where $G_T = G_I + G_{II}$.

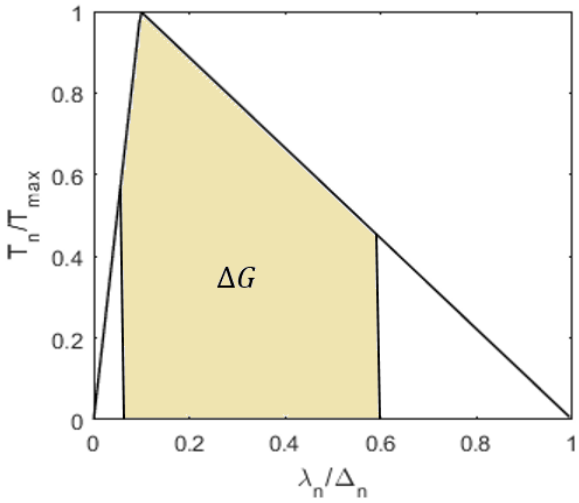

Figure 6. Illustration of energy release rate change

2.3.Implementation of fatigue law into implicit time integration

After the damage accumulation rate is determined, the fatigue damage parameter will be calculated by

$$d_{f,n+1} = d_{f,n} + \frac{\partial d_f}{\partial N} \tag{40}$$

For high cyclic loading where millions of cycles happen, it is computationally impossible to calculate fatigue damage cycle by cycle. Thus a cyclic jump method is used. It is assumed the damage accumulation rate within a range cycles are the same, then:

$$d_{f,n+m} = d_{f,n} + m\frac{\partial d_f}{\partial N} \tag{41}$$

Implicit time integration is used to reduce computational time further. The time step is taken as a relatively large value compared to loading period. If the period of the cyclic loading ΔT is the same throughout the simulation, then Equation 41 can be replaced by:

$$d_{f,i+1} = d_{f,i} + \frac{dt_i}{\Delta T}\frac{\partial d_f}{\partial N} \tag{42}$$

where i represents the count of time step. In this way, instead of applying cyclic loading, only the load envelop and load ratio R need to be provided, like shown in Figure 7. The arc-length method is used to help achieve convergence, and this is done by using the built-in algorithms in LS-DYNA. The keywords that help convergence in the input file can be found in Appendix A. Apart from the arc-length method, viscous regularization method [21] is also programmed into umat41c in LS-DYNA to help achieve convergence. In viscous regularization, a viscous damage variable d_v is introduced to replace the static damage variable d_s:

$$d_v = d_s - \eta\frac{\dot{\lambda}}{\lambda} \tag{43}$$

Where η is a viscosity and is taken as 10^{-4} in our simulation.

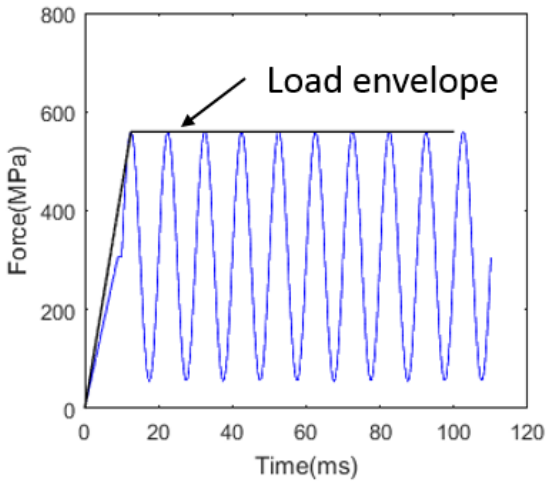

Figure 7. Cyclic loading and load envelope

3. Numerical Simulations

Two simulation verifications are presented in this section to show the feasibility of our proposed fatigue accumulation method. Both simulations are to predict the S-N curves of commonly used adhesive joints in the automotive industry. FCGR parameters for the adhesive joints in mode I and mode II are obtained from the literature, which are obtained experimentally separately by other researchers.

3.1.Single lap joint glass fiber epoxy

The first simulation is to validate the experiment done by Tang [27] on thick single lap adhesive joint to test its fatigue behavior. The adherent is glass fiber reinforced epoxy (GFRE), and the adhesive is epoxy (Figure 8). The specimen width is 25mm. It is fixed at one end and stretched at the other end under cyclic loading (Figure 9) with a load ratio $R = 0.1$ and a frequency of $5Hz$. The tensile modulus and Poisson's ratio of GFRE are summarized in Table 1 [27]. An orthotropic elastic material property is used in the simulation and shear modulus are calculated using $G_{ij} = \frac{E_i}{4(1+v_{ij})} + \frac{E_j}{4(1+v_{ji})}$ $i,j = 1,2,3$. The material properties of epoxy adhesive layer is summarized in Table 2 [28]. The critical energy release rate G_{IIC} and shear strength S are assumed to be the same as G_{IC} and T respectively, as no information is provided from paper [28]. Paris law parameters in mode I and mode II are taken from [29] and [30] respectively and are used to predict the S-N curve (Figure 10). When single lap joint is under tension, it has obvious peeling effect especially at edges, even though the adherent is very rigid. That peeling effect is verified by querying the tensile and shear stress along the adhesive joint when the tensile stress at ends are $8\ MPa$, and the stress distribution is compared to the FE simulation result (thickness=2.5mm, $y/t_a = 0.5$) in [27] , as shown in Figure 11.

Table 1. Material properties of glass fiber/epoxy composite

$E_{11}(GPa)$	$E_{22}(GPa)$	$E_{33}(GPa)$	$G_{12}(GPa)$	$G_{13}(GPa)$	$G_{23}(GPa)$	v_{12}	v_{13}	v_{23}
36.85	15.35	3.35	9.87	7.90	3.69	0.4	0.3	0.32

Table 2. Cohesive zone model parameters for adhesive layer

$G_{IC}(MPa \cdot mm)$	$G_{IIC}(MPa \cdot mm)$	$T(MPa)$	$S(MPa)$	$C1$	$m1$	$C2$	$m2$
1.69	1.69	17.7	17.7	2.25	4.85	0.104	4.16

From Figure 10 it can be observed that the S-N curve from simulation matches experiment very well. Our proposed method along with mode I and mode II Paris law parameters from the literature can predict the fatigue life of single lap adhesive joint.

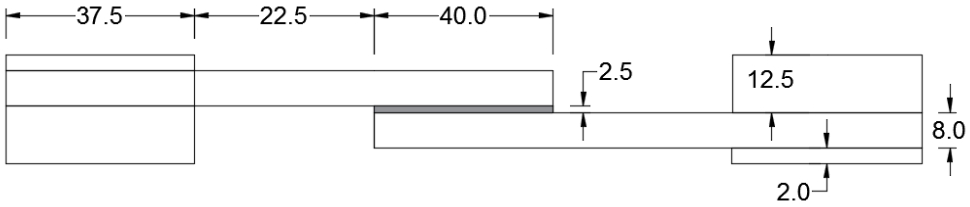

Figure 8. Geometry of GFRE single lap joint specimen

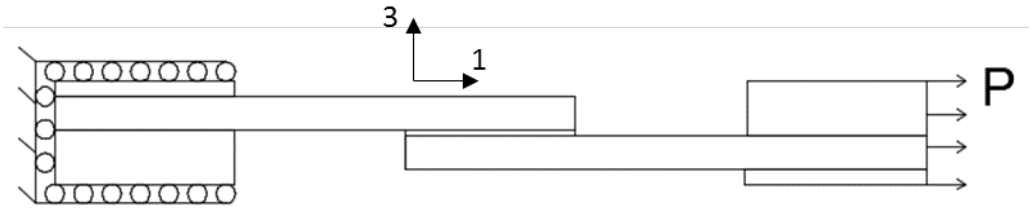

Figure 9. Load boundary condition of GFRE single lap joint specimen

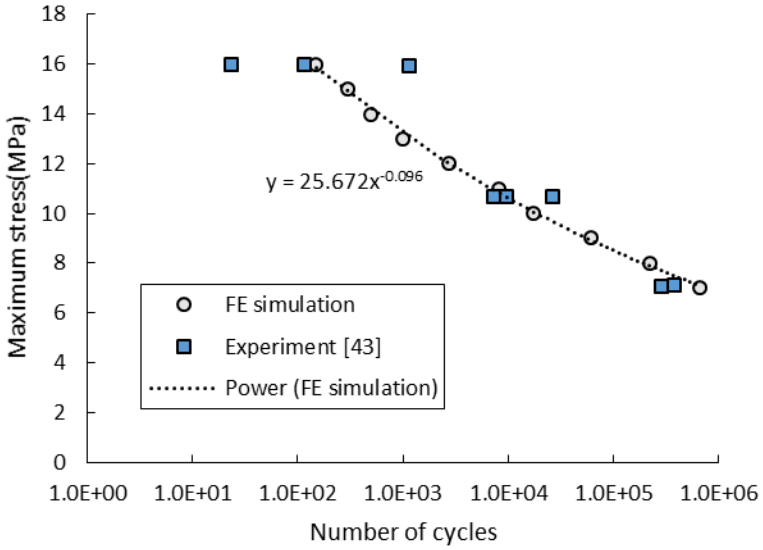

Figure 10. S-N curve of adhesive joint

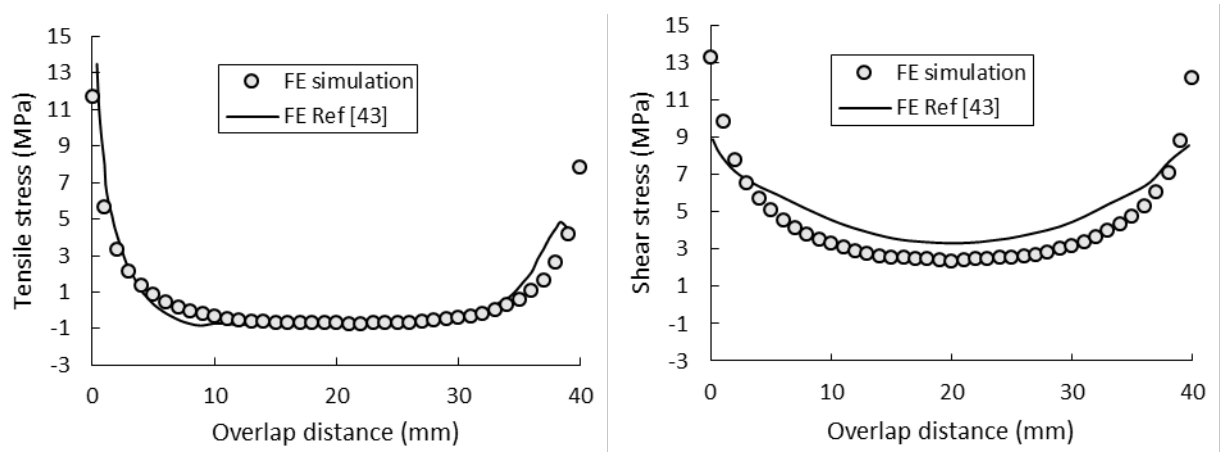

(a) (b)

Figure 11. (a) Tensile strength along the length of adhesive joint (b) Shear strength along the length of adhesive joint

3.2.Stepped lap joint carbon/epoxy

Like the previous simulation, this one is also to predict the S-N curve using FCGR, but on a stepped lap joint. The experiment is done by Kim [31]. In his paper, he studied the influence of lap length and step numbers on adhesive joint's static and fatigue strength. In our simulation, only a fixed lap length and two types of step numbers will be simulated. The two types of specimen geometry are illustrated in Figure 12, which has three steps and two steps. All the specimens have a width of 20mm. The specimens are made of carbon/epoxy composite, whose tensile modulus and Poisson's ratio are taken from [31], as shown in Table 3. An orthotropic elastic material property is used in the simulation, and shear modulus are calculated using $G_{ij} = \frac{E_i}{4(1+v_{ij})} + \frac{E_j}{4(1+v_{ji})} \quad i,j = 1,2,3.$ From [32] mode I and mode II Paris law parameters are obtained and summarized in Table 4 along with the critical energy release rate. The specimen is load at two ends in tension at a frequency of $10Hz$ and load ratio $R = 0.1$. The S-N curve data from simulation and experiment are plotted in Figure 13. Again, our method is able to predict the S-N curve very well.

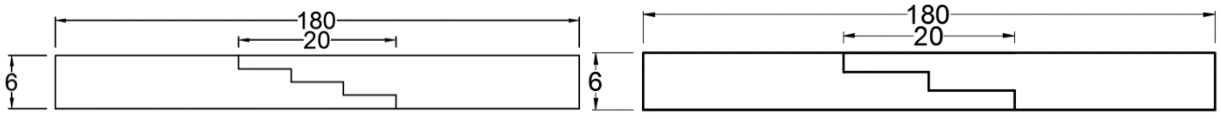

(a) (b)

Figure 12. Geometry of stepped lap joint specimen (a) 3 steps (b) 2 steps

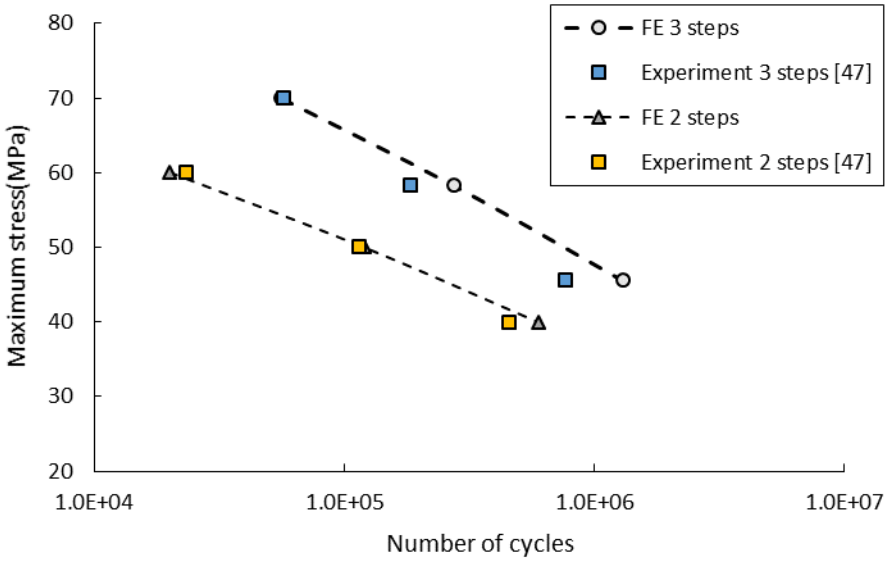

Figure 13. S-N curve of stepped lap joint

Table 3. Material properties of carbon/epoxy composite

$E_{11}(GPa)$	$E_{22}(GPa)$	$E_{33}(GPa)$	$G_{12}(GPa)$	$G_{13}(GPa)$	$G_{23}(GPa)$	v_{12}	v_{13}	v_{23}
55.1	55.1	6.24	26.24	14.3	14.3	0.05	0.08	0.08

Table 4. Cohesive zone model parameters for carbon/epoxy

$G_{IC}(MPa \cdot mm)$	$G_{IIC}(MPa \cdot mm)$	$T(MPa)$	$S(MPa)$	$C1$	$m1$	$C2$	$m2$
0.27	1.02	18.6	25.25	10.5	5.81	0.1537	4.50

4. Conclusion

A method is presented to predict the fatigue life of adhesive joints. It combines FCGR and fatigue damage accumulation in the cohesive zone model. The method calculates the fatigue damage accumulation rate using the area changes under the traction-separation curve of cohesive law. The accumulated fatigue damage is then used to reduce the strength of the cohesive zone model. The method is implemented in LS-DYNA as a user-defined cohesive material. Implicit time integration is used for high cyclic loading, and viscous regularization is applied to help achieve convergence.

The method was validated on two adhesive joints under tensile fatigue loading. One validation is to obtain the S-N curve of a GFRE single lapped joint, and the other one is to obtain the S-N curve of carbon/epoxy stepped lap joint. FCGR material parameters from the literature are used to predict the S-N curve done by separate experiments. The simulation results have good agreement with the experiment result and prove the fatigue life prediction ability of this method.

5. Appendix A. Keywords that controls convergence in LS-DYNA input file

*CONTROL_IMPLICIT_AUTO							
Iauto	Iteopt	Itewin	Dtmin	Dtmax	Dtexp	Kfail	Kcycle
1	10	10	0.0	0.1	0.0	0	0
*CONTROL_IMPLICIT_DYNAMICS							
Imass	Gamma	Beta	Tdybir	Tdydth	Tdybur	Irate	
1	0.6	0.38	0.0	1.0E28	1.0E28	0	
*CONTROL_IMPLICIT_GENERAL							
Imflag	Dt0	Imform	Nsbs	Igs	Cnstn	Form	Zero_v
1	1	2	1	1	0	0	0
*CONTROL_IMPLICIT_SOLUTION							
Nsolvr	Ilimit	Maxref	Dctol	Ectol	Rctol	Lstol	Abstol
12	6	30	0.001	0.01	1e10	0.9	1e-10
Dnorm	Diverg	Istif	Nlprint	Nlnorm	D3itctl	Cpchk	
1	1	1	0	2	0	0	
Arcctl	Arcdir	Arclen	Arcmth	Arcdmp	Arcpsi	Arcalf	Arctim
0	0	0.0	1	2	0	0	0
Lsmtd	Lsdir	Irad	Srad	Awgt	Sred		
4	2	0.0	2.0	1.0	0.0		
*CONTROL_IMPLICIT_SOLVER							
Lsolvr	Lprint	Negev	Order	Drcm	Drcprm	Autospc	Autotol
5	1	2	0	4	0	1	0
Lscpack	Mtxdmp						
2	0						

References

[1] Kadioglu F, Adams RD. Flexible adhesives for automotive application under impact loading. Int J Adhes Adhes 2015;56:73-8.
[2] Kuczmaszewski J, Bylica T. Fundamentals of metal-metal adhesive joint design. : Lublin University of Technology, 2006.
[3] Harris J, Fay P. Fatigue life evaluation of structural adhesives for automative applications. Int J Adhes Adhes 1992;12:9-18.
[4] Hadavinia H, Kinloch A, Little M, Taylor A. The prediction of crack growth in bonded joints under cyclic-fatigue loading I. Experimental studies. Int J Adhes Adhes 2003;23:449-61.
[5] Quaresimin M, Ricotta M. Fatigue behaviour and damage evolution of single lap bonded joints in composite material. Composites Sci Technol 2006;66:176-87.
[6] Pang J, Du Y, Wu K, Hu P, Li W. Fatigue analysis of adhesive joints under vibration loading. The Journal of Adhesion 2013;89:899-920.
[7] Vucko F, LeBozec N, Thierry D, Weber B, Dosdat L, Luckeneder G et al. Combined corrosion and fatigue performance of joined materials for automotive applications. Materials and Corrosion 2016;67:1143-51.
[8] Banea MD, da Silva LF. Static and fatigue behaviour of room temperature vulcanising silicone adhesives for high temperature aerospace applications. Statisches Verhalten und Dauerfestigkeitsanalyse von vulkanisierten Silikonklebstoffen für Luftfahrtanwendungen bei hohen Temperaturen. Materialwissenschaft und Werkstofftechnik 2010;41:325-35.
[9] Azari S, Jhin G, Papini M, Spelt J. Fatigue threshold and crack growth rate of adhesively bonded joints as a function of load/displacement ratio. Composites Part A: Applied Science and Manufacturing 2014;57:59-66.
[10] Du Y, Shi L. Effect of vibration fatigue on modal properties of single lap adhesive joints. Int J Adhes Adhes 2014;53:72-9.
[11] Pirondi A, Nicoletto G. Fatigue crack growth in bonded DCB specimens. Eng Fract Mech 2004;71:859-71.
[12] Roe K, Siegmund T. An irreversible cohesive zone model for interface fatigue crack growth simulation. Eng Fract Mech 2003;70:209-32.
[13] Turon A, Costa J, Camanho P, Dávila C. Simulation of delamination in composites under high-cycle fatigue. Composites Part A: applied science and manufacturing 2007;38:2270-82.
[14] Harper PW, Hallett SR. A fatigue degradation law for cohesive interface elements–development and application to composite materials. Int J Fatigue 2010;32:1774-87.

[15] Landry B, LaPlante G. Modeling delamination growth in composites under fatigue loadings of varying amplitudes. Composites Part B: Engineering 2012;43:533-41.
[16] Pugno N, Ciavarella M, Cornetti P, Carpinteri A. A generalized Paris' law for fatigue crack growth. J Mech Phys Solids 2006;54:1333-49.
[17] Dugdale D. Yielding of steel sheets containing slits. J Mech Phys Solids 1960;8:100-4.
[18] Barenblatt GI. The mathematical theory of equilibrium cracks in brittle fracture. Adv Appl Mech 1962;7:55-129.
[19] Camanho PP, Dávila CG. Mixed-mode decohesion finite elements for the simulation of delamination in composite materials. 2002.
[20] Crisfield M. An arc-length method including line searches and accelerations. Int J Numer Methods Eng 1983;19:1269-89.
[21] Yu H, Olsen JS, Olden V, Alvaro A, He J, Zhang Z. Viscous regularization for cohesive zone modeling under constant displacement: An application to hydrogen embrittlement simulation. Eng Fract Mech 2016;166:23-42.
[22] Camanho PP, Davila C, De Moura M. Numerical simulation of mixed-mode progressive delamination in composite materials. J Composite Mater 2003;37:1415-38.
[23] Benzeggagh M, Kenane M. Measurement of mixed-mode delamination fracture toughness of unidirectional glass/epoxy composites with mixed-mode bending apparatus. Composites Sci Technol 1996;56:439-49.
[24] Livermore software technology corporation. LS-DYNA keyword user's manual volume II material models. In: Anonymous ; 2013.
[25] Turon A, Camanho PP, Costa J, Dávila C. A damage model for the simulation of delamination in advanced composites under variable-mode loading. Mech Mater 2006;38:1072-89.
[26] Harper PW, Hallett SR. Cohesive zone length in numerical simulations of composite delamination. Eng Fract Mech 2008;75:4774-92.
[27] Tang J, Sridhar I, Srikanth N. Static and fatigue failure analysis of adhesively bonded thick composite single lap joints. Composites Sci Technol 2013;86:18-25.
[28] Azari S, Papini M, Schroeder J, Spelt J. The effect of mode ratio and bond interface on the fatigue behavior of a highly-toughened epoxy. Eng Fract Mech 2010;77:395-414.
[29] Brown EN, White SR, Sottos NR. Fatigue crack propagation in microcapsule-toughened epoxy. J Mater Sci 2006;41:6266-73.
[30] O'Brien TK, Johnston WM, Toland GJ. Mode II interlaminar fracture toughness and fatigue characterization of a graphite epoxy composite material. 2010.
[31] Kim J, Park B, Han Y. Evaluation of fatigue characteristics for adhesively-bonded composite stepped lap joint. Composite Structures 2004;66:69-75.
[32] Asp LE, Sjögren A, Greenhalgh ES. Delamination growth and thresholds in a carbon/epoxy composite under fatigue loading. Journal of Composites, Technology and Research 2001;23:55-68.